Electric-field induced surface instabilities of soft dielectrics and their effects on optical transmittance and scattering

Samuel Shian, Peter Kjeer, and David R. Clarke

Citation: Journal of Applied Physics **123**, 113105 (2018); doi: 10.1063/1.5018858
View online: https://doi.org/10.1063/1.5018858
View Table of Contents: http://aip.scitation.org/toc/jap/123/11
Published by the American Institute of Physics

Electric-field induced surface instabilities of soft dielectrics and their effects on optical transmittance and scattering

Samuel Shian,[a] Peter Kjeer,[b] and David R. Clarke
John A. Paulson School of Engineering and Applied Sciences, Harvard University, 29 Oxford Street, Cambridge, Massachusetts 02138, USA

(Received 10 December 2017; accepted 4 March 2018; published online 21 March 2018)

When a voltage is applied to a percolative, mechanically compliant mat of carbon nanotubes (CNTs) on a smooth elastomer bilayer attached to an ITO coated glass substrate, the in-line optical transmittance decreases with increasing voltage. Two regimes of behavior have been identified based on optical scattering, bright field optical microscopy, and confocal optical microscopy. In the low field regime, the electric field produces a spatially inhomogeneous surface deformation of the elastomer that causes local variations in optical refraction and modulates the light transmittance. The spatial variation is associated with the distribution of the CNTs over the surface. At higher fields, above a threshold voltage, an array of pits in the surface form by a nucleation and growth mechanism and these also scatter light. The formation of pits, and creases, in the thickness of the elastomer, is due to a previously identified electro-mechanical surface instability. When the applied voltage is decreased from its maximum, the transmittance returns to its original value although there is a transmittance hysteresis and a complicated time response. When the applied voltage exceeds the threshold voltage, there can be remnant optical contrast associated with creasing of the elastomer and the recovery time appears to be dependent on local jamming of CNTs in areas where the pits formed. A potential application of this work as an electrically tunable privacy window or camouflaging devices is demonstrated. *Published by AIP Publishing.*
https://doi.org/10.1063/1.5018858

INTRODUCTION

A variety of mechanical and electric-field induced deformations of the surface of soft materials, such as elastomers, can occur and are used to affect optical transmittance. For instance, under compression or with a surface layer under residual compression, an initially flat elastomer surface will wrinkle to form a rich variety of patterns, depending on the stress, the shape of the elastomer, and the boundary conditions. The simplest are periodic undulations, which can scatter light. For instance, Bowden *et al.*[1] used the residual stress created by sputtering a gold electrode on to a heated soft silicone to cause surface wrinkling upon cooling that scattered and reflected light. Wrinkling in response to a residual stress is usually irreversible and so the scattering cannot be tuned or controlled. By adding metal electrodes and using high dielectric constant soft elastomers, the wrinkling can be controlled using an electric field.[2] However, metal electrodes significantly reduce the initial transmittance of the devices to less than 40% and the lack of sharp curvatures in the sinusoidal pattern limits the light scattering angles, resulting in a low contrast ratio between the off and on state.[2] At larger strains in compression, wrinkled surfaces transition to form localized creases where the surface forms re-entrant folds.[3] Although less thoroughly studied, surface instabilities can also occur in response to electric fields applied through the thickness of a soft dielectric. Recently, we have demonstrated reversible surface roughening when an electric field is applied between a percolating nanowire electrode on one side of a thin dielectric elastomer and a planar electrode on the other side.[4] In response to the electric field, randomly distributed nanowires create inhomogeneous localized stresses that deform an initially flat surface, altering its morphology and scattering incident light by refraction.[4] Uniform surface stress, typically generated using smooth and conformal electrodes, can also induce surface deformation by way of electromechanical instability mechanisms.[2,5,6] Recently, it has been reported that at sufficiently high electric fields and using a liquid electrolyte as an electrode, the creasing becomes unstable and transitions to a periodic array of pits.[7] This pitting instability generates local deformations with a high surface curvature[8] and has been shown to be potentially useful for certain applications including control of surface adhesion[9] and optical patterning through mechano-chromism.[10] However, although the use of a liquid electrolyte as the compliant electrode is advantageous for experimentation as described in these references, it is impractical as a window device or camouflage. In this article, we use percolating single-walled carbon nanotube (CNT) mats as electrodes since they have both excellent mechanical compliance and minimal optical scattering and absorption,[11] important for optical characterization of the electric field induced surface instabilities.

In this article, we describe the correlation between electric-field induced surface instabilities and light scattering as a function of applied voltage, leading to the demonstration of an electrically tunable window device. In contrast to our previous work[12] on inducing deformation from localized stress of metallic nanowires (diameter 80 nm), this work uses CNTs (diameter

[a]Now at Solchroma Technologies, Inc., Somerville, MA 02143, USA.
[b]Deceased.

around 1 nm) to form an electrically continuous electrode and produces a uniform surface stress upon charging. The structure, shown schematically in Fig. 1(a), is a multilayer. It consists of a thin layer network of CNTs, on a soft elastomer transparent film attached to another transparent but stiffer polymer sheet, all bonded to an ITO coated glass substrate. The structure is similar to that we have described previously[4] and that utilized by Wang *et al.*[5] except that, as mentioned, they used a liquid electrolyte rather than a compliant network of CNTs as the top electrode. The glass is transparent and also mechanically constrains any lateral displacements of the elastomers produced in response to the electric field. To minimize light scattering from the interface between the two elastomer layers, both were made from the same elastomer, polydimethylsiloxane, PDMS (Sylgard 184, Dow Corning Corp.), but using a different ratio of the volume of the base elastomer and the cross-linker.

EXPERIMENTAL SECTION

The silicone elastomer (Sylgard 184, Dow Corning) dielectric layers were spun coated onto ITO coated glass substrates. The hard and soft layers were made from 10:1 and 100:2 ratios of base to cross-linker, respectively. According to the literature, the shear modulus of these compositions differs by two orders of magnitude, i.e., 700 vs. 7 kPa,[5,13] ensuring that the majority of electrically induced mechanical deformation occurs primarily within the soft layer. After each coating, the layer was cured at 120 °C for 15 min. The thickness of the stiff and the soft layers was 55 and 160 μm, respectively.

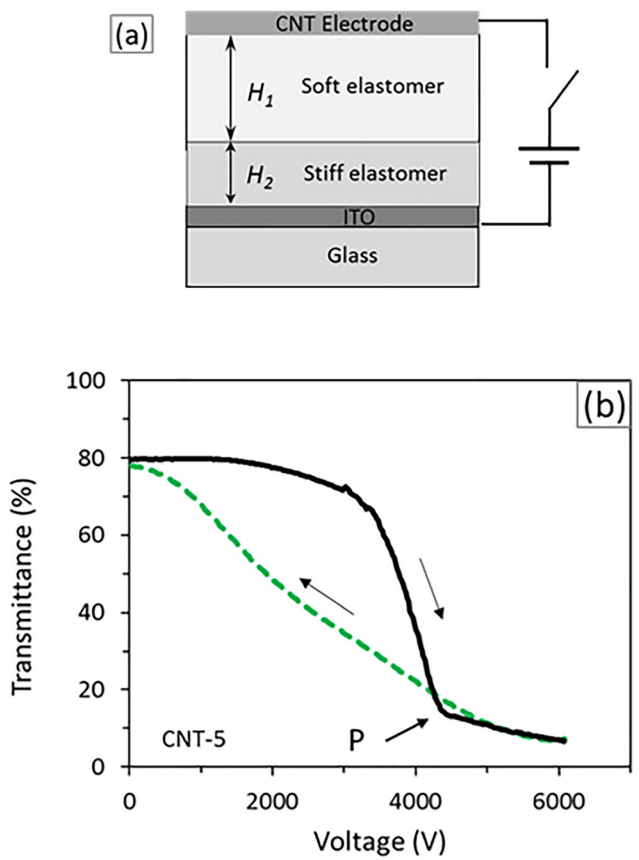

FIG. 1. (a) Schematic cross section of the multilayer structure. The compliant electrode is a percolative CNT network and the opposing electrode is an ITO coated glass with two layers of elastomer in between. The stiff elastomer, together with the underlying glass, constrains the lateral deformation of the elastomers layers when a voltage is applied. (b) The in-line optical transmittance shows a continuous transition from clear to opaque with increasing voltage (constant ramp rate of 100 V/s). The transmittance exhibits hysteresis as the voltage is increased and then reduced. The hysteresis is related to the formation of pits, their growth in size, and the subsequent collapse on removing the voltage.

The CNT electrode was prepared by either spraying or a filtration-stamping method. To prepare the stock CNT solution, hydrophilic CNT powders were purchased from a vendor (P3-SWNT, Carbon Solutions, Inc.). According to their manufacturer, the CNTs were purified with nitric acid and functionalized with carboxylic acid groups and had an average bundle diameter of 4–5 nm and length of 0.5–1.5 μm. The powder was dispersed in de-ionized (DI) water using an ultrasonic agitator (Digital 450, Branson, Danbury, CT) for 4 min at 75% power. Relatively clear dispersions of CNTs were obtained from the supernatant after centrifugation and decanting. An equal volume of iso-propanol was added to the solutions to make the stock solution for spraying. The CNTs were deposited by spraying, which is performed using a computer controlled x-y stage using a compressed-air spray gun (Model A-JU, Paasche, Inc.). In the second preparation method, the CNTs were deposited by filtration and transferred from the filter to the elastomer. In this method, the stock CNT solution was diluted using isopropanol to have an optical density of 16% transmittance for a 10 mm path length. An aliquot of the solution, typically 0.2–2 ml, was passed into a vacuum filtration apparatus having a Teflon filter (100 nm pore size and 47 mm diameter, Omnipore), leaving a CNT mat on the filter. This CNT mat was then transferred to the silicone surface by firmly pressing the sheets together to ensure complete transfer of the CNT. The Teflon filter was peeled off, leaving the CNT mat on the surface of silicone. CNT mats in varying densities were prepared and are labeled in this work according to the amount of the light absorbed by the CNT alone, excluding other layers. For example, the notation CNT-10 refers to a CNT mat electrode with an optical density that absorbs 10% of the light in transmission. It was found that there was a linear relationship between the density of the CNT and the optical absorption of the multilayer.

The angular dependence of the transmitted intensity was measured using a 2D detector in the arrangement shown in our previous work.[4] A highly collimated He-Ne laser (~1 mm diameter) was shone through the sample and detected by a 2D CMOS sensor (23.9 × 35.8 mm, model A7, Sony Corp.) placed on a translation stage, at a distance of 20 mm from the sample. The images were captured in the RAW mode at different exposure times to allow for the large dynamic range of the intensities. The pixel intensities were extracted using ImageJ software and plotted as a function of radial distance from the center of the beam. After stitching together, the data from multiple exposures of the full angular dependence was constructed. The surface morphology as a function of applied electric field was imaged using non-contact confocal microscopy with a 5× objective and a 405 nm laser source (Model OLS4000, Olympus Corp.). The

in-line spectral transmittance was measured from 400 nm to 800 nm using an Ocean Optics spectrometer with a halogen light source and a pair of collimators was used to direct the light entering and exiting the sample. The haze was measured following the ASTM standard D1003 using an integrating sphere and a reference white standard. The standard specifies that a specular transmission has a maximum spread of 2.5° and anything larger is considered to be diffusively scattered. Because of the fixed size of our collimator, we used a slightly larger spread angle of 2.9°.

RESULTS

In the absence of any voltage, the optical transmittance is close to 80% for the materials with the CNT-5 and CNT-10 electrodes. (The numbers refer to the percentage of light absorbed, which is correlated to the density of the CNT network.) The value of 80% transmittance is close to the absorption loss by the CNT and ITO layers and the surface reflectance based on the refractive indices of the elastomer and air. For a fixed density of CNT, the in-line optical transmittance decreased with increasing applied voltage and could be tuned continuously between the maximum and minimum transmittance values as shown in Fig. 1(b), as the potential was ramped up and then down at 100 V/s. With increasing voltage, the transmittance decreases with a characteristic inverted sigmoidal dependence with the majority of the decrease occurring between 3200 V and 4200 V. The actual values vary from one multilayered structure to another with a point, P, of abrupt change in the slope of the transmittance at a value of about 4000 V for this particular multilayer. The decrease in transmittance with voltage had the same dependence with successive voltage actuation cycles. On reducing the voltage from the minimum transmittance state, the transmittance increased almost linearly returning to the initial, zero voltage value, as shown by the dashed line in Fig. 1(b). Together, this leads to a transmittance hysteresis with actuation voltage which, as will be described, is related to the formation and subsequent disappearance of pits as the electric field is cycled.

With increasing applied voltage, there were corresponding changes in the elastomer surface that could be revealed by *in-situ* bright-field optical microscopy, as shown in Fig. 2. (A video recording of the changes as a function of applied voltage is included in the supplementary material, Video 1.) Before the application of any voltage, the surface is featureless except for an occasional defect, such as dust particles, for instance, one is shown in Fig. 2(a). At voltages of about

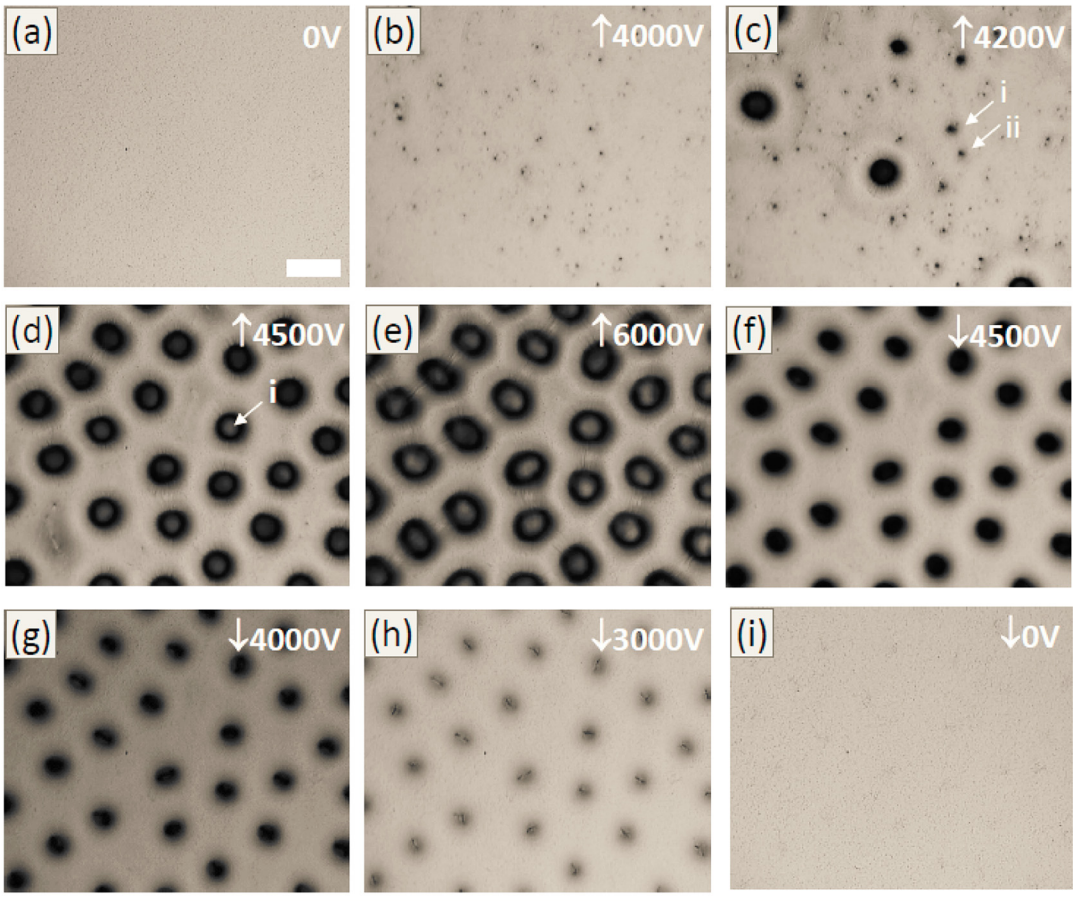

FIG. 2. Bright field optical microscope image showing the evolution of the elastomer surface as a function of voltage, labeled at the top right at each image, increasing from (a) to (e) and then decreasing (f) back to the zero voltage state (i). These images were recorded during the first actuation cycle at a voltage ramp rate of 100 V/s, using a 10× objective lens having a NA = 0.25. The bright spots in the centers of the pits in images (d) and (e) are caused by light being backscattered along the optic axis when the pit reaches the lower elastomer layer. The scale bar is 200 μm. The thicknesses of the soft and stiff elastomer layers are 55 and 160 μm, respectively.

4000 V, dark specks began to form on the elastomer surface, as shown in Fig. 2(b). In other areas, small creases also became visible the image. At this voltage, as can be seen in the transmittance curve of Fig. 1(b), the direct transmittance had dropped to about half. At 4200 V, some of the specks suddenly grew to become the large, dark circular features seen in Fig. 2(c). Based on geometrical optics, decreases in optical intensity in the bright field image are associated with increasing proportion of light being scattered back at an angle exceeding the angle subtended by the objective aperture. These circular features correspond to the "craters" identified by Wang *et al.*[5] At the voltage at which the pits appeared, the transmittance curve typically exhibits a kink, as indicated by the arrow P in Fig. 1(b). With still further increases in the applied voltage, the areal number density of the pits abruptly increases, as illustrated in the microscope images (Fig. 2), and as quantified in Fig. 3(a). This voltage, which spans the nucleation and growth of the pits, is very similar to the voltage at which the transmittance kink occurs. Concurrently, the transmittance further decreases towards a low saturation value corresponding to a minimum transmittance. The average spacing between the pits also decreases rapidly in this voltage range and then becomes almost constant, independent of the voltage [Fig. 3(b)]. The apparent size of the pits also grows while maintaining an approximately circular outline until, at the highest voltages, they impinge and their outlines become more pronounced and irregular in shape, as illustrated in Fig. 2(e).

Despite these dramatic changes in the apparent size and number density of pits, there is relatively little change in the in-line transmittance in this regime and most of the changes in transmittance occur well before the pits nucleate. Subsequently, when the voltage is reduced, the size of the individual pits steadily decreases until none are distinguishable while the number density of the pits remains approximately constant, as seen in the series of micrographs in Figs. 2(f)–2(i). However, there is a remaining optical contrast, barely discernable in the first actuation sequence images but more pronounced with repeated actuation, of rather indistinct features at the same locations that the pits were visible at maximum voltage. The identity of these features is not known but it is observed that when the voltage is again ramped up, the majority of the pits appear to preferentially re-nucleate at or near these sites. The hysteresis and the continuous linear increase in transmittance as the voltage is decreased to zero are consistent with the existence of pits that decrease in size until the voltage reached zero. The average spacing between the pits was $\sim 200\,\mu$m, similar to but slightly greater than the thickness of the soft elastomer layer ($\sim 160\,\mu$m).

Detailed examination of the bright-field images reveals several other interesting features. For instance, pits can nucleate and grow at pre-existing "defects," such as the dust particles. There is also evidence for competitive growth of the pits with increasing voltage, for instance some small adjacent but undeveloped pits form, as is illustrated by features (i) and (ii) in Fig. 2(c), but then one (i) grows at the expense of its neighbors. We also observe that, in contrast to the observations of Wang *et al.* who used ionic liquid electrodes, the pits do not form a regular, close-packed arrangement. We attribute this to inhomogeneities in the spatial

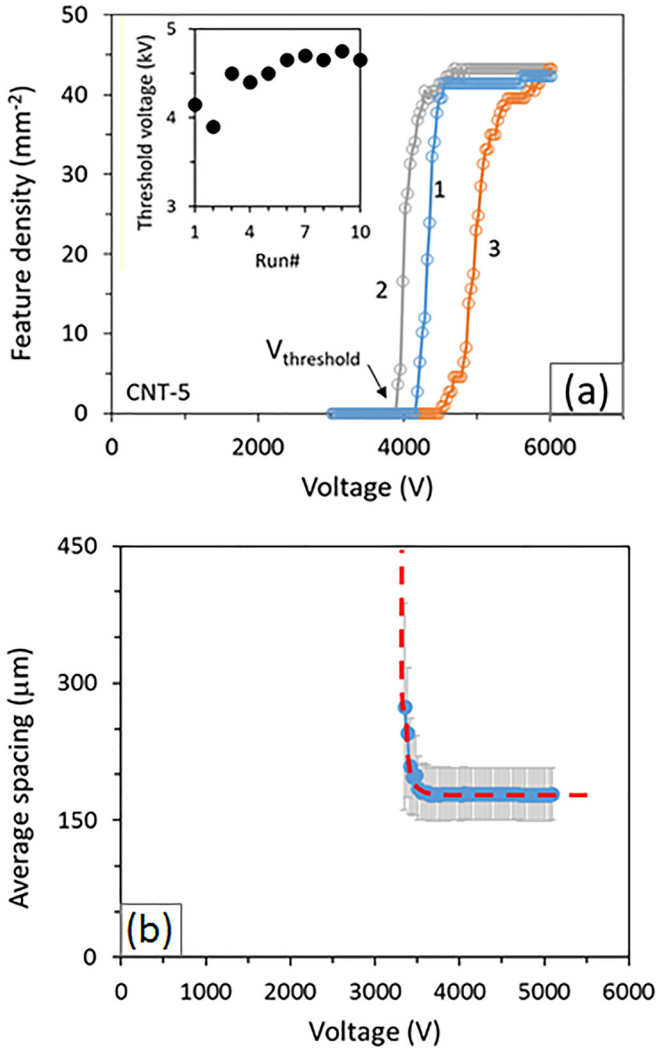

FIG. 3. (a) Number density of pits as a function of voltage for successive actuation cycles. The inset shows the variation in threshold voltage for the nucleation of pits with actuation cycling. (b) Average spacing between pits as a function of voltage.

distribution in CNT and correspondingly in the electric field, in particular at the ends of the individual CNTs.

With increasing number of voltage actuation cycles there are also some changes in the pits. The first is that the threshold voltage for the formation of pits varies in the first few cycles but then increases slightly before stabilizing, for this particular multilayer, at around 4600 V, as seen in the inset in Fig. 3(a). In spite of this variation, the number density of pits nevertheless remains constant. However, the location of the individual pits can also change from cycle to cycle. Although, the majority renucleate at the same locations as they were in the preceding actuation cycle, the relative location of the individual pits can change appreciably over a large number of actuation cycles. This can be seen in Fig. 4 where the position of the pits in cycle #1 and cycle #2 are highly correlated [compare Figs. 4(a) and 4(b)]. However, comparing the images, for instance those in the first and tenth cycle [Figs. 4(a) and 4(f)], the details of the local configurations can be distinguished. The third change is that the shape of some of the pits become progressively elongated with increasing number of actuation cycles, as illustrated by those arrowed in Figs. 4(a)–4(c). The

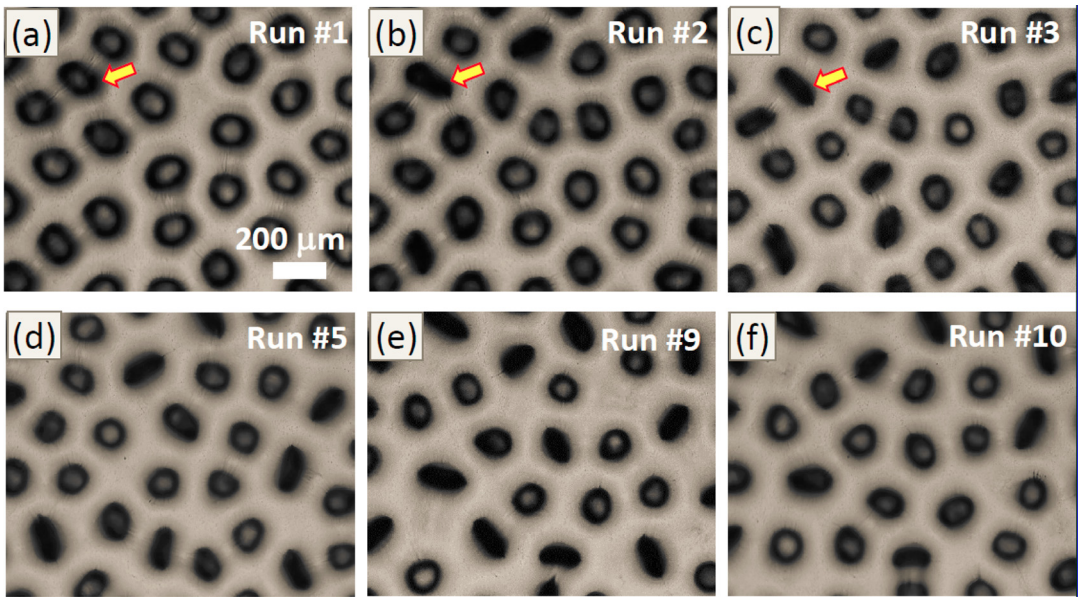

FIG. 4. Snapshots of the pitting at 6 kV at the same location for sample CNT-5 with increasing number of actuation cycles from the first cycle in (a) to the tenth cycle in (f). Some changes in the pits at different actuation cycles are visible from these snapshots including the location, the shape, and size of some pits.

proportion of elongated pits also increases with cycling. Concurrently, the remnant shape of the pits at zero voltage, not shown here, becomes more elongated, forming a line or crease at high cycle numbers as will be shown in Fig. 5.

More detailed morphological information comes from *in-situ* confocal microscopy. This reveals that these elongated remanent shapes are creases that grow wider and deeper but maintain the same length, with increasing voltage, as can be seen in Figs. 5(a) and 5(b). Then, above the threshold voltage, pits typically form at one or other end of each crease, as indicated by the one arrowed (i) in Fig. 5(d). A line profile along the creases indicates that the peak-to-valley depth of the crease appeared to vary continuously as the voltage increases, as seen in Fig. 5(e) and plotted in Fig. 5(f) along with the optical transmittance of this particular multilayer sample (CNT-10). It is notable, as shown in Fig. 5(e), that height variations exceeding the wavelength of light are created at a voltage of 2500 V just as the transmittance is

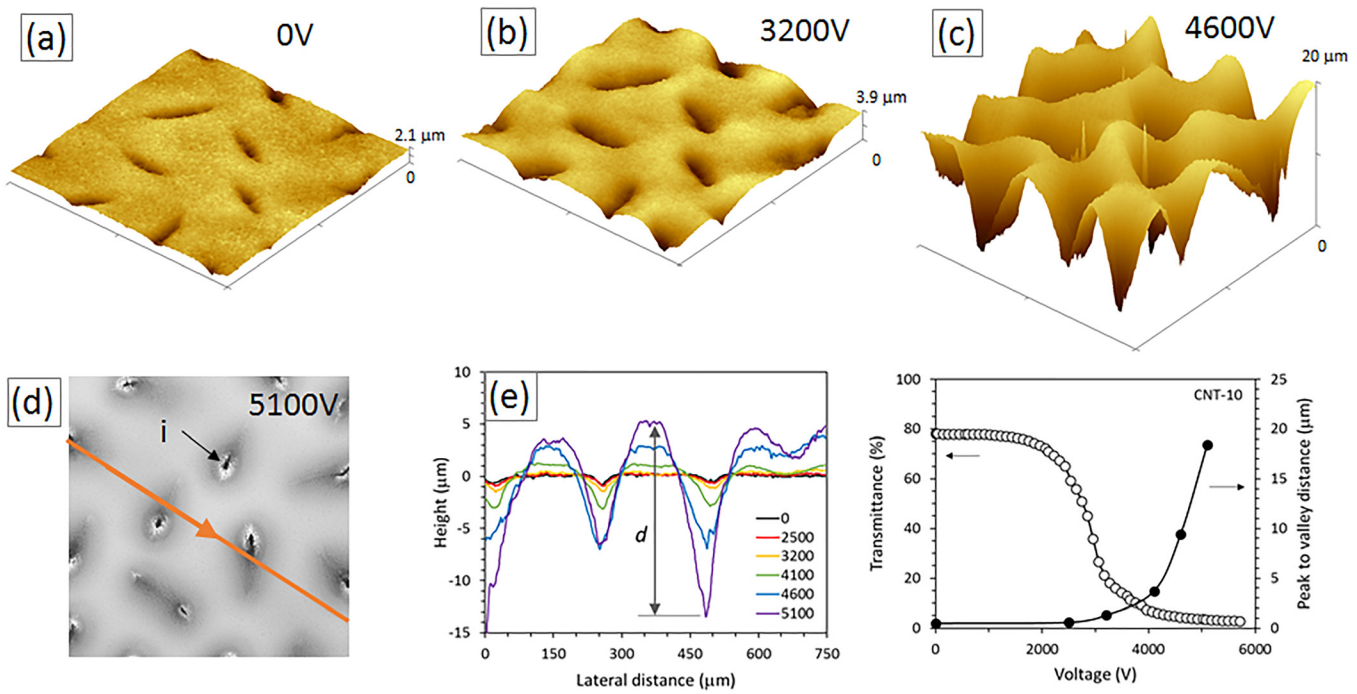

FIG. 5. (a)–(c) Confocal microscope images show the evolution of the surface with increasing voltage. Unlike Fig. 2, this sample had been actuated many times prior to recording these images. Sample CNT-10 and a scanned area of 836 × 836 μm^2. (d) Surface height image in which the dark areas indicate lower elevation. The white "halos," arrowed, are imaging artifacts. (e) The height variation along the line shown in (d) at the different actuation voltages indicated. With increasing voltage deep pits form in the elastomer while the displaced material pushes up in between (e). The peak to valley depth, d, together with the in-line transmittance as a function of voltage in (f).

beginning to decrease. Figure 5 also suggests that, once formed, the pits are conical in shape. Furthermore, the displaced volume produced as pits form in the elastomer is accommodated by an increase in height of the surface in between. This progressive increase in surface height between pits is shown in Fig. 5(e). [We note that confocal microscopy has limitations on the maximum slope detectable; above the limit, the area with a steep slope is erroneously inverted, and becomes pointed up as seen by the spike artifacts in Fig. 5(c) and the white area artifacts surrounding the pits in Fig. 5(d).]

The optical scattering was quantified from measurements of the angular spread of a collimated laser beam shone through the multilayer as a function of the actuation voltage. An example is shown in Fig. 6(a), which compares the scattering from the intrinsic surface roughness of the elastomer itself, the additional scattering from the CNT electrode and the scattering at voltages of 4, 5, and 6 kV. In the absence of the CNTs, the angular distribution is indistinguishable from

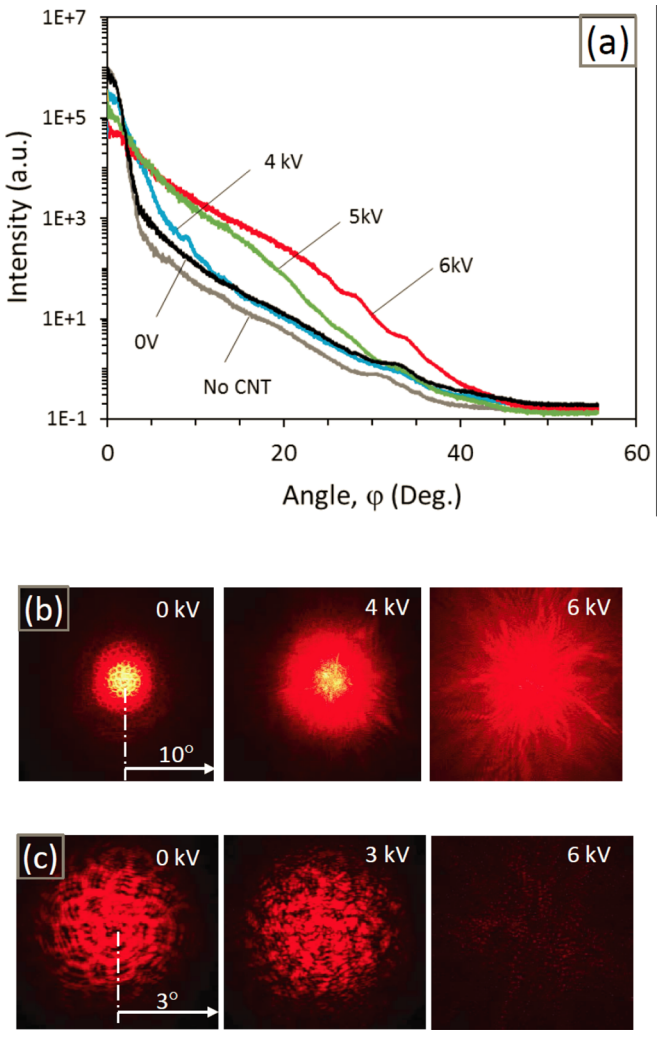

FIG. 6. (a) Angular distribution of the transmitted laser beam (632 nm) through the multilayer structure CNT-10. The broadening increases substantially as the surface deforms in response to the increasing electric field. The recorded images of the transmitted beam as a function of voltage are shown at two different angular magnifications and exposures: (b) 1/80 s and (c) 1/8000 s. The patterns at 0 kV are the projection of the surface creases formed by plastic deformation of the soft elastomer layer occurring after multiple actuation cycles. The threshold voltage of the onset of pitting for CNT-10 was approximately 4.5 kV.

that of the laser beam itself, with most of its intensity confined within ±5°. The integrated intensity of the peak (<5°) is the in-line transmission in Fig. 1(b). The angular scattering from the CNT is very similar but with a slightly higher intensity at all angles greater than ±5°. At a voltage of 4 kV, the angular profiles became broader at the expense of the in-line intensity but only out to angles <15° while the higher angle (>15°) scattering intensity remained unchanged. Upon further increasing the voltage to 5 kV, the angular scattering broadened to an angle of ±35° and the in-line intensity further decreased. At 6 kV, the peak intensity had decreased by more than an order of magnitude, while the intensity at high angles increases by a similar amount to ∼30°. Although these scattering observations are similar to those of our previous work using silver nanowires instead of CNTs, we noticed that for the case of silver nanowires, the intensity of the angular distribution of the beam increases uniformly at all angles as the voltage increases, rather than being limited below a certain angle as in this case.[14] More intriguing is that close examination of the image of the transmitted laser beam after actuation and return to the zero-voltage state reveals that the transmitted beam has a complex structure, shown in Figs. 6(b) and 6(c) at different angular magnifications. Although the detailed origin of the fine structure is not fully understood, it is attributed to the presence of remnant creases where the local surface has not yet fully relaxed. With increasing voltage, the structure within the transmitted beam becomes less distinct, the beam spot broadens and, concurrently, the in-line intensity (the center part of the beam) diminishes. The blurring suggests overlapping of the refraction effects as the creases and pits produce larger curvatures with increasing voltage.

Complementary variations in optical haze occurred as a function of applied voltage, Fig. 7(a). In the absence of any voltage, the haze depends on the areal density of CNT used to form the electrode as well as the surface roughness of the elastomer. For the electrode used for the transmittance measurements in Fig. 1(b), the intrinsic haze for CNT-10 was 2.5% and this did not significantly change until a voltage of 2000 V. Thereafter, it increased nonlinearly with voltage. We note that the onset of the voltage-dependent haze occurs at approximately the same voltage as the transmittance begins to decrease but well before the pits begin to form.

DISCUSSION

Comparison between the optical transmittance data, the optical micrographs, and the confocal images, shows there are two distinct and reversible mechanisms that affect light transmittance as a function of applied voltage. The first, at low electric fields, is attributed to the surface deformation in the vicinity of the CNTs produced by the local electromechanical (Maxwell) stress producing spatially varying optical refraction.[4] The second mechanism occurs at higher fields and is associated with the formation of three-dimensional, approximately conical, pits in the surface. This also produces optical refraction effects but of greater complexity due to the more complicated three-dimensional shape

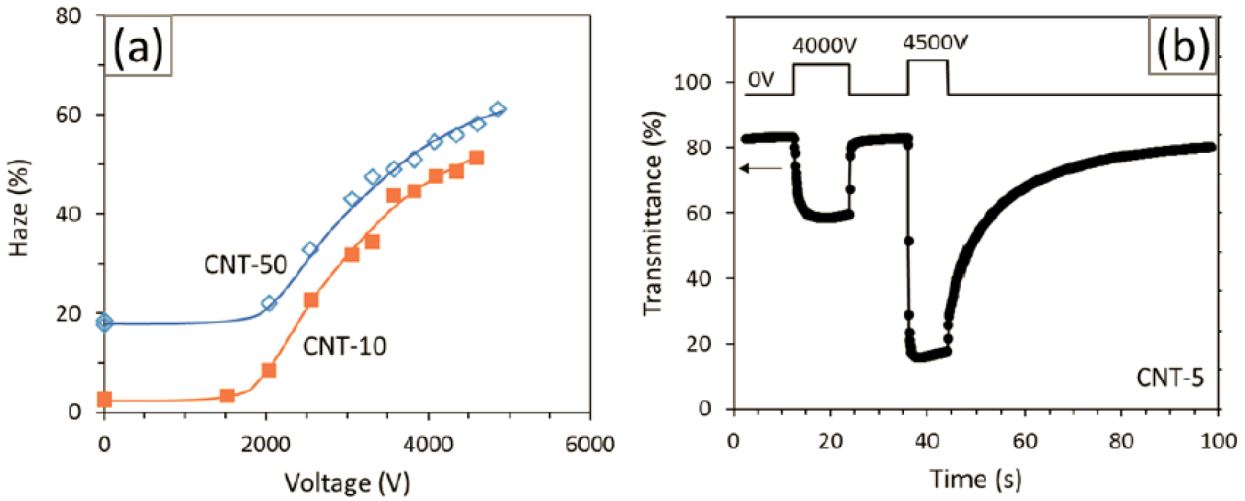

FIG. 7. (a) The haze as a function of actuation voltage for two different CNT electrode densities. (b) The time dependence of the optical transmittance when electrical pulses at two different voltages are applied, one below and one above the threshold voltage, 4300 V for this particular multilayer. The data was recorded at intervals of 0.2 s.

produced by the longer range collective surface instability in the elastomer in response to the higher electric fields.

In the lower field regime, wherein the majority of the change of the in-line transmittance occurs with increasing applied voltage, the optical scattering and the decrease in the in-line transmittance is most likely associated with the local deformation of the elastomer surface produced by the electrostatic attraction between the individual nanotubes of the CNT mat electrode and the underlying flat electrode. We conclude this based on observations of our previous work with silver nanowires[4] where displacements of the elastomer surface around the individual nanowires as a function of voltage, as well as the silver nanowires themselves, could be observed directly. In that work, we also showed that the intensity of the angular scattering calculated from measured height profiles as a function of applied voltage, by geometric optics, using Lumerica's FDTD software, was in good agreement with the measured variations in angular scattering with voltage.

As the diameter of the CNTs is significantly smaller than that of the nanowires and is also non-reflective, we have not been able to resolve the spatial variation in surface deformation about individual CNTs but the changes in angular scattering data indicate that the surface deforms in a similar manner. Once a threshold voltage is exceeded, pits form by a nucleation process and subsequent rapid growth in both the number density and size. The value of the nucleation voltage is difficult to identify with any precision as pits nucleate at random over the surface of the elastomer but as shown in Fig. 3, it is possible to identify a threshold voltage at which the number density rapidly increases with a small increase in voltage. It should be emphasized, though, that the major changes in the optical transmittance actually occur at voltages lower than the threshold voltage at which the pits form [Figs. 1(b) and 5(f)]. Despite the dramatic changes in optical contrast observed in the optical microscope at the onset of pit formation, the contrast changes are exaggerated due to imaging using a microscope with a high numerical aperture, specifically the acceptance angle of a microscope objective lens aperture being much larger than that of the collimating lenses used to determine the in-line transmittance. Consequently, the optical microscope collects the scattered light from the deformed elastomer surface at all angles up to its acceptance angle. In addition, because of auto brightness-contrast mechanisms in the camera software, microscope images are also more sensitive to spatial variations in contrast than to the overall intensity, further emphasizing the contrast. Returning to the effect of the pits on the optical transmittance, the confocal microscopy profiles recorded once the voltage exceeds the threshold voltage, could be used to calculate the in-line transmittance and the angular scattering intensity using geometric optics. Although relatively straight forward to do so, we have not done so since the confocal profiles [Fig. 5(e)] indicate that the angle that the pit walls are very large (60°–80°) and are rather variable, meaning that the pit surfaces scatter to large angles well outside the line of direct transmission.

For soft dielectrics that deform under electric field, local thinning such as the formation of a pit, can cause catastrophic dielectric breakdown that occurs at a lower electric field than the nominal breakdown field.[15] In reality, however, the high electric field at the bottom of the pit reaches or exceeds the dielectric breakdown strength of the material. In a single layer of soft material, the instability, i.e., the positive feedback between the Maxwell force and the electric field extends the depth of the pit controllably. The use of two layers of dielectrics, soft and stiff, limits the depth of the pit to within the thickness of the soft layer as the stiff layer is relatively undeformed. This configuration enables the device to sustain the high electric field that drives the formation of pits throughout the surface of the soft dielectric.

Although the pits form rapidly, they disappear more slowly when the field is reduced, typically of the order of tens of seconds for the elastomer films we used. Once formed, though, they are effective in scattering light but as their number density does not decrease with decreasing voltage and only their size, it can be concluded that the linear decrease in transmittance, shown in Fig. 1(b), is directly related to the projected area of the pits. So, it is likely that

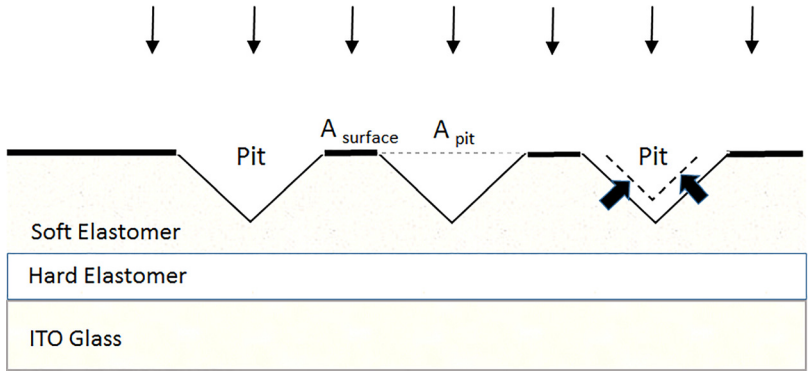

FIG. 8. Schematic of the cross-section between a row of pits. The total light transmitted depends on the total flat area of the surface, $A_{surface}$, whereas the amount scattered depends on the projected area of the pits. Microscopy observations indicate that the pits shrink linearly (arrowed) and so, consequently, the transmittance increases approximately linearly with decreasing voltage until they disappear when the voltage is reduced to zero.

once formed, light is refracted by both the detailed shape of the pits and, in between them, from the local distortions around the individual CNTs themselves (the first mechanism). Nevertheless, we can see the overall effect of such deformation in the slight darkening in the elastomer surface as illustrated in Fig. 2(b). After the pits form and stabilize in number, the pits grow in size at increasing voltage, as can be seen by comparing Figs. 2(d) and 2(e). These indicate that the extent of deformation also increases and consequently increases the scattering by the elastomer, as seen by the decreasing rate of the optical transmittance at high voltages.

Additional insights come from the response times when the voltage is turned on and off. Although elastomers are known to be viscoelastic, there is a marked difference in the response times for two voltage pulses, one below the threshold voltage (∼4300 V), and the other above [Fig. 7(b)]. Below the threshold voltage, the transmittance decreases and reaches a constant value plateau faster during relaxation than that during turn-on. However, above the threshold voltage the opposite occurs in which the turn-on response (<1 s) is significantly faster than the relaxation time (∼20 s). Such a difference in the response times below and above the threshold field is inconsistent with a simple visco-elastic mechanical response. Two possible explanations for the slow relaxation response above the threshold voltage can be envisaged. One is that a larger quantity of charge is injected and then trapped within the elastomer at the higher voltages. The other is that the jamming of the CNTs in the vicinity of the pits retards the viscoelastic response. Detailed experiments will be needed to determine the origin of this unexpected response behavior.

Based on our observations, the physical picture of the nucleation, growth, and subsequent collapse of the pits that emerges is as follows: with increasing applied voltage, there is a threshold field at which isolated pits form heterogeneously at random on defects at the surface or within the soft layer. Although, these defects can be dust particles, impurity particles, or sub-micron voids, it is most likely, based on the large electric field concentrations attainable at sites of high local curvatures that they mainly form at the ends of the CNTs. With increasing number of actuation cycles, it can also be at the end of creases remaining from the preceding actuation. With increasing voltage, there is rapid nucleation of more pits and their growth in size over the entire surface of the soft elastomer. These rapidly grow in size and depth until they penetrate down well below the surface, possibly to the surface of harder elastomer underneath. At the same time, they interact with one another to form an approximately close-packed arrangement. The formation of the pits requires surface distortion, local bending, and stretching of the CNT mat, as well as mass flow of the elastomer under the electric field. This is evidenced by the volume of the pits, imperfectly captured by the confocal measurements of the pit shapes, and the uplift of the elastomer surface in between the pits. When the applied voltage is decreased from its maximum value, our observations (Fig. 2) indicate that the pit number density remains constant while the size of the pits decreases steadily until disappearing when the applied voltage is reduced to zero. This coincides with the observed, approximately linear increase in optical transmittance as the voltage is decreased as shown in Fig. 1(b) until the transmittance returns to the zero-voltage value. Assuming that the walls of the pits refract light away from the transmitted beam and the shape of the pits remains similar as they shrink, the transmittance will change linearly with the areal fraction of almost flat areas in between pits, as shown schematically in Fig. 8.

Not captured by our observations, because of the lack of requisite resolution, the compliant electrode mat of CNTs over the pits is likely to also be deformed locally as it is attached to the elastomer surface. The increase in the length of the line profile extracted from the confocal image [Fig. 5(e)] suggests that the surface area of the elastomer increases through stretching as the voltage increases. In particular, the center of pits experiences the largest stretching and the deformation radially decreases. It is speculated that the remnant contrast after the voltage is reduced to zero is due to the plastic deformation of the surface associated with the relatively large deformation and the jamming of the CNTs as the elastomer elastically recovers when the field is removed. Specifically, as the pits form, the CNTs have to slide past one another to follow the increase in the surface area and when the pits shrink, the CNT network has to deform back to the flat surface. Implicitly, the rate at which the CNT network can recover its initial configuration will depend on the extent of the local deformation produced by the pitting and the viscosity of the elastomer. If they cannot do this

FIG. 9. (a)–(d) A demonstration of light scattering is shown by the change in the opacity to objects placed behind a multilayered device with increasing voltage. The flowers, the blue ball, and the booklet were placed behind the elastomer device, at distances 25 cm, 100 cm, and 150 cm, respectively.

completely, the jammed CNT can hold the faces of the pit open to form the creases seen in the confocal images and the residual optical contrast. As the center of the pits deform the most, these remnant creases are most visible in the area where the center of pits once formed [see the faint marks in Fig. 2(i)]. As different silicone elastomers exhibit different relaxation times, depending on their electrical and mechanical characteristics,[16] the time taken for the creases to close will be dependent on the particular elastomer.

One particularly intriguing observation is shown in Fig. 4 illustrating that the spatial location where individual pits nucleate, and grow, does not remain identical on voltage cycling above the threshold voltage. The identity of the nucleating sites is not known but it is presumed that pits nucleate at the ends of individual CNTs belonging to percolating clusters once the local electric field at the tip of the CNT exceeds a critical value. The observation that the pits do not always re-nucleate at the same place suggests two possible explanations or a combination of the two. One explanation is that the end of the nucleating CNT is burnt away by the local charge flow needed to create the pit so another CNT subsequently serves as a nucleation site when the voltage is next applied. This is consistent with observations of "soft" breakdown that can occur when CNT networks are used as electrodes in dielectric elastomers and polymer capacitors. A second explanation is that the local stretching of the elastomer surface that occurs when the pits form may cause thinning of the CNT mat or local redistribution of the CNTs attached to the elastomer causing the CNT responsible for pit nucleation to move to another location or for another, nearby CNT to serve as the nucleation site when voltage is re-applied.

Finally, to illustrate the utility of the instabilities as an electrically tunable light diffuser, objects located at different distances were imaged as shown in Fig. 9(a). These objects, including flowers, a blue ball, and a booklet, are located at successively larger distances of 30, 100, and 150 cm, behind the device. At zero voltage, the multilayer is highly transparent and the individual objects are seen clearly. With increasing voltage, the image became increasingly hazy and at a voltage of 5000 V, the objects could no longer clearly be seen. Upon the removal of voltage, the transparency of the device returns to its initial state. The transition to hazy occurs relatively quickly, in less than 2 s, however, the return transition occurs at a slower rate, at tens of seconds. The switching speed and the reproducibility of the transition are shown by the real-time Video 2 in the electronic supplementary material. The switching speed of the transition is affected by several factors, including the resistance of the electrodes, the overall capacitance of the device, and the viscoelasticity of the elastomer, none of which has been optimized in the current work. These contributions will be described and quantified in a future publication.

CONCLUSIONS

In summary, voltage-induced surface instabilities of a soft elastomer layer are strongly correlated with decreases in optical transmittance. At small voltages, the surface roughens by local surface displacements produced as individual carbon nanotubes are attracted to an oppositely charged planar electrode, the ITO coated glass. At higher voltages, the roughening increases and is attributed to instabilities akin to creasing. At still higher voltages, the surface undergoes a strongly coupled electro-mechanical instability to form an irregular array of pits that are believed to extend through the thickness of the soft-elastomer layer. These electric field induced microstructural changes are reversible, although the recovery time can, in the case of pitting, be quite long and depends on both the elastomer and the local geometrical configuration of the CNT electrode.

SUPPLEMENTARY MATERIAL

See supplementary material for the following videos: (1) Video recording of the nucleation and growth of electric-field induced pits with increasing applied voltage and the subsequent shrinkage and disappearance as the voltage is decreased back to zero. Real time. (2) Demonstration of the use of the voltage induced opacity in a window application with three objects at different distances behind the window. Figure 9 is taken from this video sequence.

ACKNOWLEDGMENTS

This work was supported by the National Science Foundation through Grant No. CMMI-1333835 and in part by the NSF MRSEC Program Award No. DMR 14-20570.

[1]N. Bowden, S. Brittain, and A. Evans, "Spontaneous formation of ordered structures in thin films of metals supported on an elastomeric polymer," Nature **393**, 146–149 (1998).
[2]D. van den Ende, J.-D. Kamminga, A. Boersma, T. Andritsch, and P. G. Steeneken, "Voltage-controlled surface wrinkling of elastomeric coatings," Adv. Mater. **25**, 3438–3442 (2013).
[3]M. Das, A. Vaziri, A. Kudrolli, and L. Mahadevan, "Curvature condensation and bifurcation in an elastic shell," Phys. Rev. Lett. **98**, 014301 (2007).
[4]S. Shian and D. R. Clarke, "Electrically-tunable surface deformation of a soft elastomer," Soft Matter **12**, 3137 (2016).
[5]Q. Wang, L. Zhang, and X. Zhao, "Creasing to cratering instability in polymers under ultrahigh electric fields," Phys. Rev. Lett. **106**, 118301 (2011).
[6]N. Arun, A. Sharma, P. S. G. Pattader, I. Banerjee, H. M. Dixit, and K. S. Narayan, "Electric-field-induced patterns in soft viscoelastic films: From long waves of viscous liquids to short waves of elastic solids," Phys. Rev. Lett. **102**, 254502 (2009); N. Wu and W. B. Russel, "Micro- and nano-patterns created via electrohydrodynamic instabilities," Nano Today **4**, 180–192 (2009); E. Schaffer, T. Thurn-Albrecht, T. P. Russell, and U. Steiner, "Electrically induced structure formation and pattern transfer," Nature **403**, 874–877 (2000).
[7]Q. Wang and X. Zhao, "Beyond wrinkles: Multimodal surface instabilities for multifunctional patterning," MRS Bull. **41**, 115–122 (2016).
[8]Q. Wang, X. Niu, Q. Pei, M. D. Dickey, and X. Zhao, "Electromechanical instabilities of thermoplastics: Theory and *in situ* observation," Appl. Phys. Lett. **101**, 141911 (2012).
[9]B. Xu and R. C. Hayward, "Low-voltage switching of crease patterns on hydrogel surfaces," Adv. Mater. **25**, 5555–5559 (2013).
[10]Q. Wang, G. R. Gossweiler, S. L. Craig, and X. Zhao, "Cephalopod-inspired design of electro-mechano-chemically responsive elastomers for on-demand fluorescent patterning," Nat. Commun. **5**, 4899 (2014).
[11]S. Shian, R. M. Diebold, E. McNamara, and D. R. Clarke, "Highly compliant transparent electrodes," Appl. Phys. Lett. **101**, 061101 (2012); S. Rosset and H. R. Shea, "Flexible and stretchable electrodes for dielectric elastomer actuators," Appl. Phys. A **110**, 281–307 (2013).
[12]S. Shian and D. R. Clarke, "Electrically tunable surface deformation of a soft elastomer," Soft Matter **12**, 3137 (2016).
[13]I. D. Johnston, D. K. McCluskey, C. K. L. Tan, and M. C. Tracey, "Mechanical characterization of bulk Sylgard 184 for microfluidics and microengineering," J. Micromech. Microeng. **24**, 035017 (2014).
[14]S. Shian and D. R. Clarke, "Electrically tunable window devices," Opt. Lett. **41**(6), 1289–1292 (2016).
[15]J. Blok and D. G. Legrand, "Dielectric breakdown of polymer films," J. Appl. Phys. **40**, 288–293 (1969).
[16]F. B. Madsen, A. E. Daugaard, S. Hvilsted, and A. L. Skov, "The current state of silicone-based dielectric elastomer transducers," Macromol. Rapid Commun. **37**, 378–413 (2016).